Q. J. R. Meteorol. Soc. (2006), **132**, pp. 467–483 doi: 10.1256/qj.05.25

Life cycles of North Atlantic teleconnections under strong and weak polar vortex conditions

By KATRIN WALTER and HANS-F. GRAF†
Max-Planck-Institute for Meteorology, Hamburg, Germany

(Received 21 February 2005; revised 12 October 2005)

SUMMARY

This paper investigates the role of the strength of the polar stratospheric winter vortex in the dynamics of the life cycles of North Atlantic teleconnections. A new set of teleconnection patterns was produced from low-pass-filtered daily 300 hPa height data of NCEP (National Centers for Environmental Prediction) reanalysis data 1958–1998. All teleconnections are meridional dipoles, which to a certain degree resemble the North Atlantic Oscillation based on surface pressure data. There are two distinct teleconnections (one over the eastern and one over the western North Atlantic) during episodes of weak polar vortex, and only one, over the central North Atlantic, during strong polar vortex episodes. The teleconnections have periods of about two weeks. Stream function tendency analysis of the life cycles shows that the relatively simple resulting teleconnections evolve from very complex structures. During the growth phase of the teleconnection indices there are strong and systematic differences between the two polar vortex regimes. While in the weak vortex regime the anomaly growth is mainly driven by transient eddy vorticity fluxes from the low-frequency domain, in the strong vortex regime there is also low-frequency advection of relative vorticity resulting from the interaction of low-frequency eddies with stationary eddies.

KEYWORDS: North Atlantic Oscillation Polar vortex

1. INTRODUCTION

The dominant lower tropospheric teleconnection pattern in the North Atlantic sector is the North Atlantic Oscillation (NAO, Wallace and Gutzler 1981). It strongly influences winter surface air and sea surface temperature over wide regions of the North Atlantic Ocean, Eurasia and the Mediterranean, the Arctic and North America. Fluctuations of the NAO are also associated with changes in the strength and direction of the North Atlantic storm tracks and, thus, with changes in precipitation over Europe and the Mediterranean (for an overview see Hurrell *et al.* 2003). Normally the temporal variability of the NAO is defined by the difference in surface pressure between the two atmospheric centres of action involved, the Icelandic Low and the Azores High. Different datasets were used in the past to construct time series of the NAO index. While for the northern part of the oscillation generally station data from Iceland are applied, the southern part sometimes is identified with data from the Azores, sometimes from Lisbon or Gibraltar at the south-west of the Iberian Peninsula. The alternative use of these station data may also include differences in the structure of the underlying teleconnection pattern and, hence, obscure the dynamical processes behind it. Structural changes in the North Atlantic Oscillation might also have a strong impact on the atmospheric variability in a large part of the northern hemisphere (Castanheira *et al.* 2002). Such modifications can be induced by a strong polar vortex acting on the vertical propagation characteristics of tropospheric planetary waves (Charney and Drazin 1961; Perlwitz and Graf 1995). Structural changes of the leading tropospheric variability patterns (which closely resemble the NAO patterns) were identified based on a separate analysis during strong and weak stratospheric polar vortex regimes (Castanheira and Graf 2003). Perlwitz and Graf (2001) showed that reflection of stationary planetary wave (zonal wave number one) energy takes place when the polar vortex exceeds a critical

† Corresponding author: Centre for Atmospheric Science, Cambridge University Geography Department, Downing Place, Cambridge CB2 3EN, UK. e-mail: hfg21@cam.ac.uk
© Royal Meteorological Society, 2006.

threshold in the lower stratosphere. Recently, Perlwitz and Harnick (2003) provided evidence for planetary wave reflection having a dependence on upper stratospheric wind shear. Perlwitz and Harnik (2004) suggested that during times of a weak polar vortex a direct link exists between stratosphere and troposphere via downward propagating zonal mean anomalies. This downward propagation of a signal takes the order of two weeks from the upper stratosphere to the mid troposphere (Perlwitz and Harnick 2004). In the case of a strong vortex, the link becomes indirect and acts via the reflection of wave energy, which has its origin in the troposphere. While the direct effect is a slow process lasting in the troposphere for monthly to seasonal time-scales, the indirect effect is faster and its time-scale compares with that of the NAO.

The NAO is basically a barotropic oscillation and hence has the best signal-to-noise ratio in the upper troposphere. The time-scale of the life cycle of the NAO is 10 days to two weeks (Feldstein 2003) and this is the time-scale we will concentrate on in this study. Hence, we will focus on the indirect effect discussed by Perlwitz and Harnick (2004). The results of Kodera and Kuroda (2004) suggest that this indirect effect may be superposed on a more zonal effect reflecting the Arctic Oscillation and including the pressure fields over the North Pole and Mediterranean. Whether or not this is an expression of the direct effect cannot be judged within this study and remains an interesting question for further research.

Using reanalysis data of the 300 hPa height, Walter and Graf (2005) defined three new dominating North Atlantic Teleconnection (NAT) indices for the middle to upper troposphere, one for the strong (NAT-SVR) and two for the weak polar vortex regime (western and eastern NAT-WVR) (see their Figure 1), and suggested that the 'classical NAO pattern' at the surface is a blend of these three new NAT patterns. They used a teleconnectivity analysis (Wallace and Gutzler 1981) and index time series were constructed for the eastern (65°–70°N, 27.5°–35°W and 37.5°–40°N, 15°–22.5°W) and western (62.5°–65°N, 77.5°–82.5°W and 35°–37.5°N, 55°–62.5°W) NA-WVR patterns, and for NA-SVR (55°–60°N, 30°–45°W and 30°–35°N, 35°–45°W) using the difference of normalized geopotential height anomalies at the southern and northern centres of action of the respective teleconnection pattern. A positive index then stands for an enhanced north–south geopotential height gradient. The stream function patterns related to these indices are shown in Fig. 1. They are clearly separated. The correlation between the eastern and western NAT-WVR monthly mean indices is only 0.41. Correlations are much smaller at the time-scale of the NAO (∼2 weeks), which is also the time-scale of the NAT. Then eastern and western NAT-WVR indices are correlated with $r = 0.18$, indicating linear statistical independence and, hence, two separate teleconnections if the polar vortex is weak.

Walter and Graf (2005) argued that storm tracks and precipitation anomalies and their relation to the phase of the dominating NAT pattern index depend on the regime of the polar stratospheric vortex in winter. The NAO index is correlated to the NAT indices, but by no means perfectly. While the monthly mean eastern NAT-WVR pattern index is highly correlated (0.91) with a 'classic' NAO index based on sea-level pressure over Iceland and the Azores, the western NAT-WVR index (0.62) and the NAT-SVR (0.74) index are much less, although still significantly, correlated with the NAO index. Walter and Graf (2005) interpreted these significant correlations mainly as a result of spatial overlapping of the patterns and of temporal averaging. Even the correlation patterns of sea surface temperatures of the North Atlantic Ocean with indices of the respective NAT change significantly between different polar vortex regimes (Graf and Walter 2005). However, so far these results are merely based on statistical analyses and remain mainly descriptive with respect to the dynamics behind the changes.

The current paper concentrates on the tropospheric variability in the North Atlantic region and the teleconnections associated with it at time-scales below one month. The dynamics leading to build-up and decay of anomalies of the NAT indices and the contributions from single forcing terms are studied by means of the tendency of the stream function (Cai and van den Dool 1994). The analysis is an extension of the work of Feldstein (2003) since it separates the data into strong and weak polar vortex regimes and focuses on a new set of NATs. A caveat concerning this analysis is the restricted amount of available reanalyses, leading to relatively weak statistical significance after double separation of the data. It is planned to repeat this study with long model control runs in order to increase the available data and improve statistical significance.

2. Data and methods of analysis

We used daily mean reanalysis data of geopotential height from the National Centers for Environmental Prediction/National Center for Atmospheric Research (NCEP/NCAR; Kalnay *et al.* 1996) for the winter months December to March from 1958 to 1998. The mean annual cycle was removed from the data. Since the data are not completely homogeneous due to changes in the density and quality of observational input (e.g. the introduction of satellite information in 1979) we did not study trends. These were eliminated by subtraction of ten-year running means. The reanalysis data in the northern hemisphere extratropics provide fairly accurate information also in the upper troposphere (Kistler *et al.* 2001).

We adopted the thresholds of the zonal-mean zonal wind at 65°N at 50 hPa of >20 m s^{-1} for the strong and <10 m s^{-1} for the weak polar vortex regime from Castanheira and Graf (2003) and defined 71 months as SVR and 32 months as WVR. Index time series calculated from low-pass-filtered (Blackmon and Lau (1980) 10-day low-pass filter) 300 hPa geopotential height were used for the following examinations.

The stream function is defined as the inverse Laplacian of relative vorticity. In the quasi-geostrophic framework, stream function ψ and geopotential height z are related by $\psi = g \cdot f^{-1} \cdot z$, where g is the gravitational acceleration and f the Coriolis parameter. Forcing mechanisms involved in the growth and decay of the teleconnection anomalies are examined by analysing the low-frequency stream function tendency equation term by term. Following the procedure applied by Cai and van den Dool (1994) and Feldstein (1998), the low-frequency stream function tendency equation can be written as

$$\frac{\partial \psi}{\partial t} = \sum_{1}^{8} \chi_i + R \tag{1}$$

with the residual R and the single terms representing the forcing by advection of planetary vorticity:

$$\chi_1 = \nabla^{-2}(-\mathbf{v}^{\mathrm{L}} \cdot \nabla f), \tag{2}$$

by advection of (relative) vorticity due to the interaction of low-frequency eddies with the zonal-mean part of the time-mean flow:

$$\chi_2 = \nabla^{-2}(-[\overline{\mathbf{v}}] \cdot \nabla \xi^{\mathrm{L}} - \mathbf{v}^{\mathrm{L}} \cdot \nabla[\overline{\xi}]), \tag{3}$$

by advection of (relative) vorticity due to the interaction of low-frequency eddies with the zonally asymmetric part of the time-mean flow, i.e. with the stationary eddies:

$$\chi_3 = \nabla^{-2}(-\overline{\mathbf{v}^*} \cdot \nabla \xi^{\mathrm{L}} - \mathbf{v}^{\mathrm{L}} \cdot \nabla \overline{\xi^*}), \tag{4}$$

by the low-frequency contribution to the divergence term:

$$\chi_4 = \nabla^{-2}\{-(f+\overline{\xi})\nabla\cdot\mathbf{v}^{\mathrm{L}} - \xi^{\mathrm{L}}\nabla\cdot\overline{\mathbf{v}}\}, \tag{5}$$

by transient-eddy vorticity fluxes:

$$\chi_{\mathrm{tr}} = \nabla^{-2}\{-\nabla\cdot(\mathbf{v}'\xi')\}^{\mathrm{L}} \tag{6}$$

and by vertical vorticity advection and tilting terms:

$$\chi_8 = \nabla^{-2}\left(-\mathbf{k}\cdot\left\{\nabla\times\left(\omega^{\mathrm{L}}\frac{\partial\mathbf{v}}{\partial p} + \overline{\omega}\frac{\partial\mathbf{v}^{\mathrm{L}}}{\partial p} + \omega'\frac{\partial\mathbf{v}'}{\partial p}\right)\right\}\right)^{\mathrm{L}}. \tag{7}$$

ψ represents the stream function, ξ the relative vorticity, and $\mathbf{v}$ the horizontal wind vector (u, v), where u is the zonal and v the meridional component. ω is the vertical wind component, a the Earth's radius, and f the Coriolis parameter. An overbar denotes a time mean; primes indicate deviations from the time mean, square brackets indicate a zonal mean, and an asterisk a deviation from the zonal mean. The superscripts $^{\mathrm{L}}$ and $^{\mathrm{B}}$ represent low pass (>10 days) and band pass (2.5–6 days) filtered quantities, respectively.

In order to separately determine the influence of synoptic and low-frequency fluctuations, the unfiltered variables v' and ξ' in term χ_{tr} (Eq. (6)) were filtered in time with the Blackmon and Lau (1980) band-pass and low-pass filters. Fluctuations with periods between 2.5 and 6 days and with periods longer than 10 days are analysed. Thus, synoptic and low-frequency fluctuations are well separated. Hence, term χ_{tr} can be split into forcing contributions from low-frequency eddy vorticity fluxes:

$$\chi_5 = \nabla^{-2}\{-\nabla\cdot(\mathbf{v}^{\mathrm{L}}\xi^{\mathrm{L}})\}^{\mathrm{L}}, \tag{8}$$

from band-pass-filtered (synoptic) eddy vorticity fluxes:

$$\chi_6 = \nabla^{-2}\{-\nabla\cdot(\mathbf{v}^{\mathrm{B}}\xi^{\mathrm{B}})\}^{\mathrm{L}} \tag{9}$$

and from mixed terms describing the interaction between the low-frequency and the synoptic eddies:

$$\chi_7 = \nabla^{-2}\{-\nabla\cdot(\mathbf{v}^{\mathrm{L}}\xi^{\mathrm{B}}) - \nabla\cdot(\mathbf{v}^{\mathrm{B}}\xi^{\mathrm{L}})\}^{\mathrm{L}}. \tag{10}$$

The residual R originates from fluctuations that are not captured by the filtered data. It includes physical processes that are neglected, such as external forcing and dissipation. R also contains errors in the balance, e.g. arising from the use of daily-mean data. Additional errors result from the computation of the total stream function tendency with centred differences in time. It turns out that R is generally very small compared to the other components.

3. Results

The patterns of the 10-day low-pass-filtered 300 hPa stream function regressed linearly onto the index time series of the three North Atlantic Teleconnection (NAT) patterns are presented in Fig. 1. The Figure clearly shows the basically dipolar structures of the teleconnection patterns. The correlation with the index time series exceeds ±0.8 in both centres of action. The NAT-SVR pattern has an additional weak maximum over eastern Europe (Fig. 1(c)). This secondary maximum has the same sign as the anomaly at the southern centre of action, but the amplitude is only half as large. The correlation

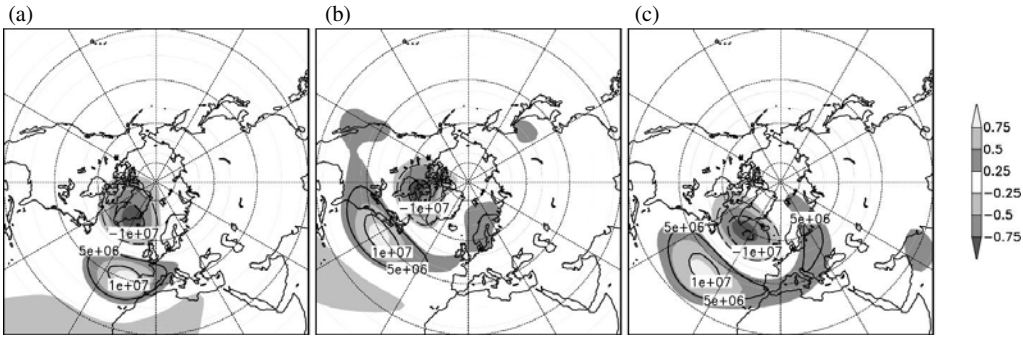

Figure 1. Linear regression coefficient (m^2s^{-1} isolines) of the 10-day low-pass-filtered 300 hPa stream function at each grid point regressed onto the index time series of (a) the eastern NAT-WVR pattern, (b) the western NAT-WVR pattern and (c) the NAT-SVR pattern. The shadings display the correlation coefficients. The regression coefficients correspond to one standard deviation of the respective index time series and are calculated only with data from the vortex regime in which the teleconnection index is defined.

with the NAT-SVR teleconnection index is less than 0.4. A secondary maximum over northern Europe can also be observed for the western NAT-WVR pattern Fig. 1(b), but it is even weaker than for the NAT-SVR pattern and the stream function anomaly does not exceed 5×10^6 m^2s^{-2}.

For the following examination of life cycles, persistent episodes with either very high or low teleconnection index values have to be categorized. In this study, an episode with positive NAT index values is defined as persistent if the index exceeds 0.75 standard deviations (σ) for at least 5 days. The examination of the life cycles focuses on the growth phase of the anomalies. Thus, episodes had to be selected in which the anomalies really grow and are not already large at the beginning of the episode. We therefore introduced the following constraint: the index values must be smaller than 0.5 σ for at least 5 days before the onset day, i.e. the day before the index becomes larger than 0.75 σ. For episodes with negative index values the procedure is analogous but with the limits $-0.75\,\sigma$ and $-0.5\,\sigma$. If there are two such episodes within 20 days, the case with the stronger increase or decrease of index values on the onset day is chosen. The thresholds were selected such that only very large persistent episodes are captured and that the number of the selected episodes is not too small. The shortness of the available reanalysis data period is a general problem, which might be overcome by using model data in a future study. For the current study we note that the datasets are relatively small and so the results are to be treated with caution. Nevertheless we think that the main differences between the two polar vortex regimes are so clear that they will be also robust.

To display the growth or decay of the teleconnection patterns, the low-pass-filtered 300 hPa stream function field was projected onto the regression patterns in Fig. 1. Before this, the regression patterns were standardized by division with the (spatial) root-mean-square value over all grid points. Figure 2 shows composites of such projections. The projections range from 10 days before to 10 days after the onset day. The thick lines represent the average over all persistent episodes, i.e. over 30 positive or 23 negative NAT-SVR index episodes and over 9 (10) positive or 12 (12) negative eastern (western) NAT-WVR index episodes. The grey lines display the average plus or minus one standard deviation. In all cases, the average projections start with values of opposite sign and reach their largest values 3–5 days after the onset day. It takes 6–8 days from crossing the zero line to reach the maximum values. While the absolute timing

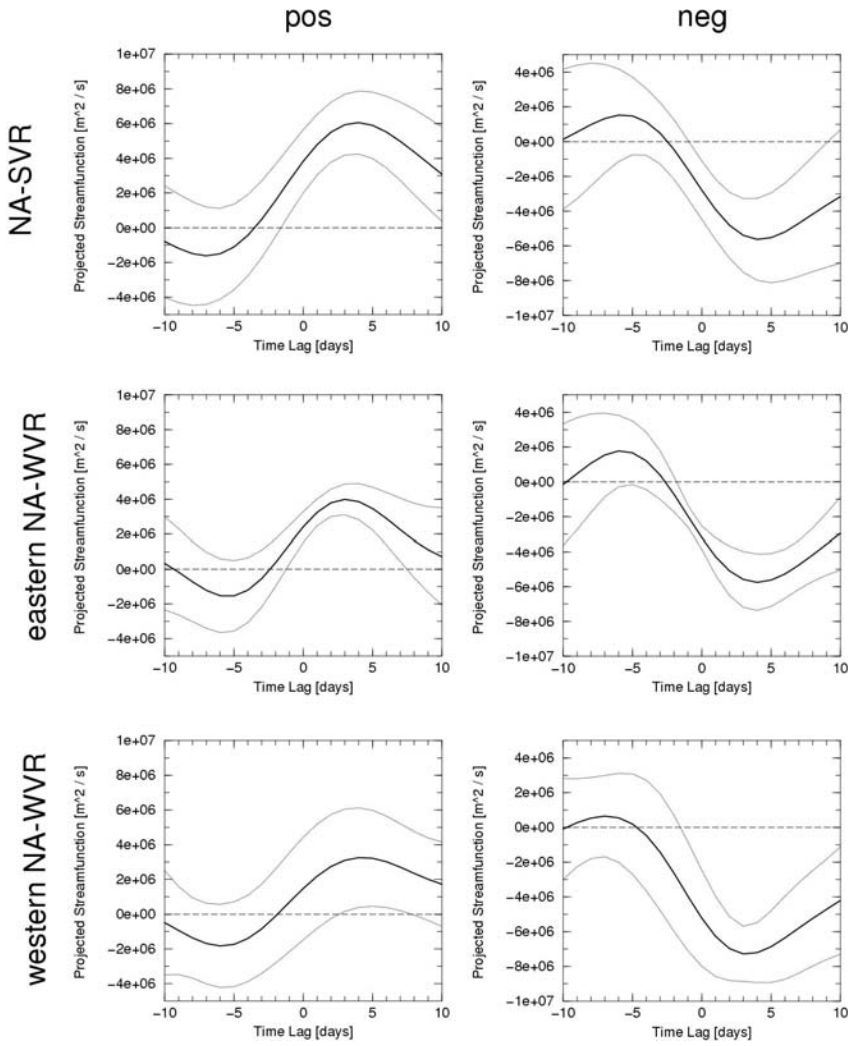

Figure 2. Projection of the 10-day low-pass-filtered 300 hPa stream function anomaly fields (m^2s^{-1}) onto the standardized regression patterns in Fig. 1. The solid lines display the composite projection for the persistent anomalies defined in the text, the grey lines the composite plus/minus one standard deviation. Shown are composites for positive (left column) and negative (right column) events of the NAT-SVR (upper row), the eastern NAT-WVR (middle row) and the western NAT-WVR pattern index (lower row).

is dependent on the selection process for the episodes studied, the relative timing is not. Hence the sequence of processes contributing to build-up or decay of the anomalies is not affected by the selection of the episodes. The interpolated average duration of such persistent episodes thus amounts to about two weeks and is comparable with the results of Feldstein (2003) for the NAO. The amplitudes of the NAT-SVR fluctuations are almost equal in both polarities, whereas for the NAT-WVR patterns, the composite amplitudes during the negative phases are larger than during the positive phases. However, an inspection of the corresponding composite stream function fields (not shown) revealed that these differences are only gradual. The spatial structures are almost identical for both polarities of the respective teleconnection pattern and similar to the regression patterns in Fig. 1. The decay of the averaged anomalies seems to be less rapid

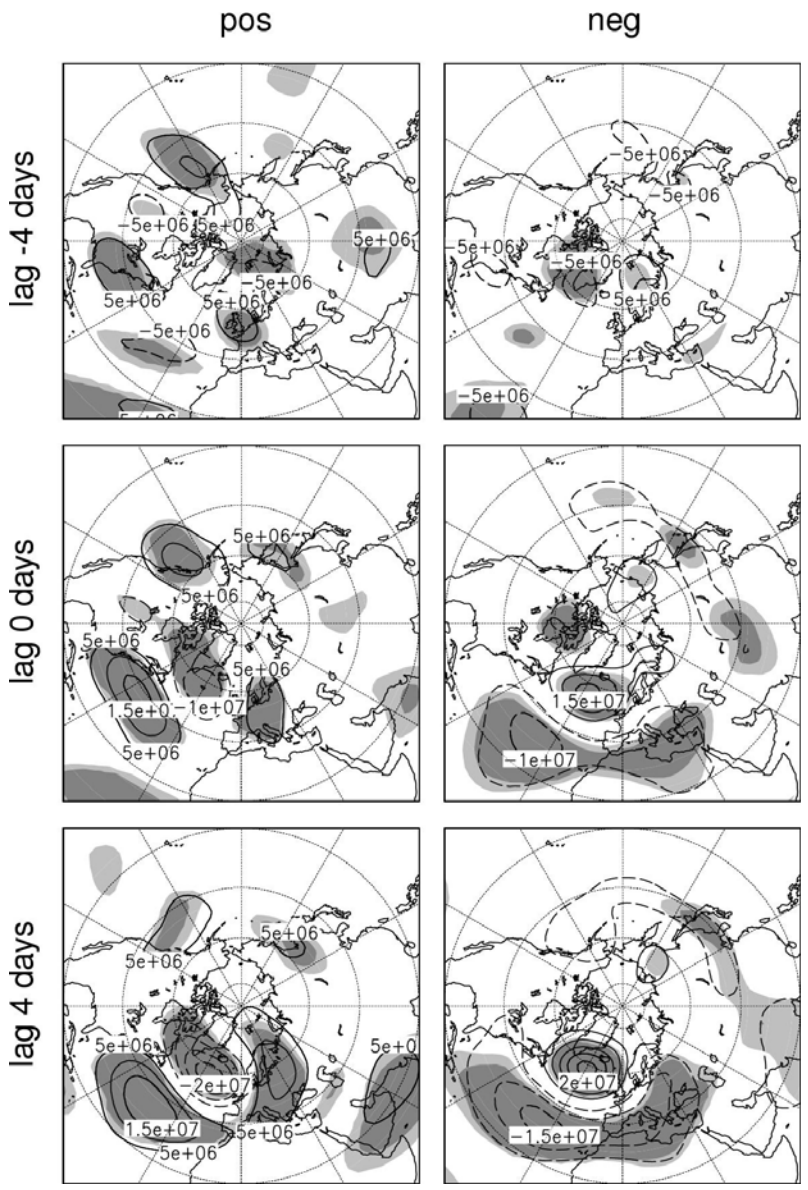

Figure 3. Composite low-pass-filtered 300 hPa stream function (m^2s^{-1}) at different time lags for the positive (left panels) and negative (right panels) persistent NAT-SVR pattern index episodes. Upper row: lag −4 days; middle row: lag 0 days; lower row: lag 4 days. The shadings indicate that the t-test significance of the anomalies is above 95% (light shading) or 99% (dark shading).

than their growth. This is a consequence of composition based on the onset day, which favours rapid growth on that day (Feldstein and Lee 1996). Another consequence of this procedure is that the standard deviation of the projections is smaller close to the onset day than for longer time lags. The focus of the following examinations will be on the growth phase, i.e. when the standard deviations are smallest.

Figure 3 shows composites of the low-pass-filtered 300 hPa stream function anomaly for positive and negative NAT-SVR pattern index events at different time lags.

Only weak anomalies can be identified in the North Atlantic sector, 4 days before the onset day (Fig. 3, upper row). The structure of the teleconnection pattern does not emerge at that time. Instead, there are weak positive (negative) stream function anomalies over the subpolar North Atlantic and negative (positive) ones over the subtropics for the positive (negative) index events. This reflects the previous finding that the composite projection onto the standardized regression pattern (Fig. 2, upper row) is weak but of opposite sign several days before the onset day. The sign of the anomalies is changed on the onset day (Fig. 3, middle row). The anomaly structures over the North Atlantic are then similar to the regression patterns. The anomalies grow until they reach their maximum values 4 days after the onset day (Fig. 3, lower row).

The positive phase of the NAT-SVR pattern, at least until the onset day (lag 0), seems to be connected with a wave train across North America, but there is no such link either in the negative phase of the NAT-SVR pattern or for both polarities of the eastern NAT-WVR pattern (not shown). In his examination of NAO lifecycles, Feldstein (2003) also described a connection with such a wave train only for the positive phase of the NAO, but he found nothing like this in the negative NAO phase. He did not, however, study differences between polar vortex regimes. The left panels of Fig. 3 suggest that a positive stream function anomaly (a 'high') moves eastward, starting at the North American east coast and expanding during the positive NAT-SVR pattern events. This, however, is not the case for the negative index events, in which the anomalies expand eastwards from an almost fixed position in the central North Atlantic. There is no indication for such distinctly moving anomalies in the NAT-WVR pattern composites (not shown). For all patterns and polarities, however, the maximum growth phase is characterized by almost fixed structures identical to the regression patterns in Fig. 1. Therefore, the differences in the initial stream function patterns at the very beginning of the growth phase will not be discussed any further in this study.

In the following, projections of the stream function tendency and of single terms in Eq. (1) onto the standardized regression patterns (Fig. 1) are discussed. Figure 4 shows the projections for positive (left) and negative (right) NAT-SVR index events. The maximum stream function tendency and, thus, the most rapid growth of the low-frequency anomaly can be observed 1 to 2 days before the onset day. Figure 4 shows that the forcing contribution from term χ_8, i.e. from the sum of the vertical vorticity advection and tilting terms, is very small throughout the whole life cycle and can therefore be neglected. Most of the stream function tendency is explained by the terms χ_1 to χ_4 and χ_{tr}. This implies that the error in the imperfectly balanced budget in Eq. (1), the residual R, is substantially smaller than the sum of the other terms. The projections for the two NAT-WVR patterns are qualitatively similar to those for the NAT-SVR pattern in Fig. 4 and are therefore not shown.

Figures 4(c) and (d) show that term χ_4 (black dashed lines), the low-frequency contribution to the divergence term, is mainly responsible for the decay of the low-frequency stream function anomalies. The projection reaches its largest value several days after the onset day, i.e. when the stream function anomaly is also large. This is not only true for the NAT-SVR but also for the NAT-WVR projections (Fig. 5). Feldstein (2003) argued that the low-frequency divergence term χ_4 is associated with Ekman Pumping. Figures 4(c) and (d) and Fig. 5 furthermore show that, in each case, the projection of term χ_4 starts with values of the opposite sign before the low-frequency stream function anomaly develops. The reason is that, before the actual anomaly develops, the stream function tendency field is characterized by (small) anomalies of opposite sign (Fig. 3). The divergence term acts to destroy them. Transient-eddy vorticity fluxes (term χ_{tr}) contribute much towards the growth of the stream function

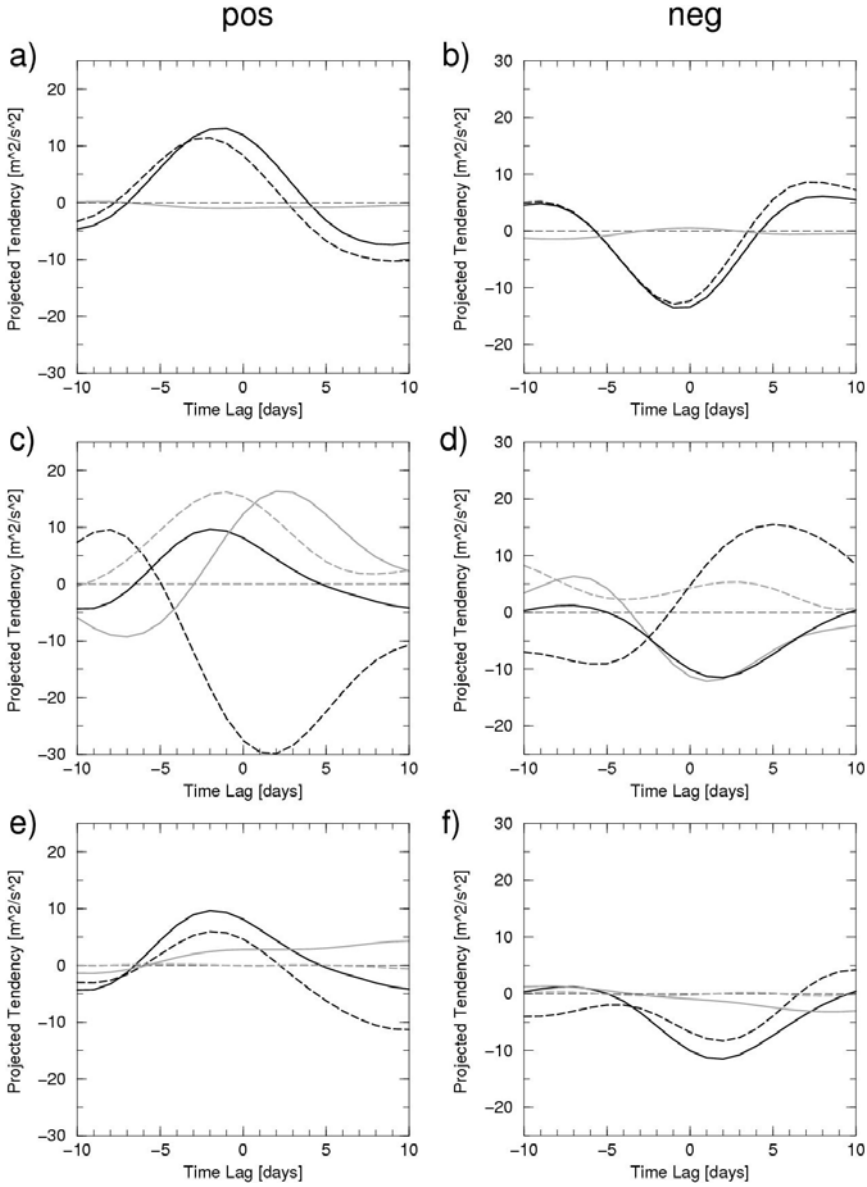

Figure 4. Projection of the 10-day low-pass-filtered 300 hPa stream function tendency and single terms of Eq. (1) ($m^2 s^{-2}$) onto the standardized regression patterns (Fig. 1) for the positive (left panels) and negative (right panels) persistent NAT-SVR pattern index episodes. Upper row: projection of the stream function tendency (black solid line), the sum of terms χ_1 to χ_4 and χ_{tr} (black dashed line), and term χ_8 (grey line). Middle row: projection of term χ_{tr} (black solid line), χ_4 (black dashed line), χ_3 (grey solid line) and the sum of terms χ_1 and χ_2 (grey dashed line). Lower row: projection of term χ_{tr} (black solid line), χ_5 (black dashed line), χ_6 (grey solid line) and χ_7 (grey dashed line).

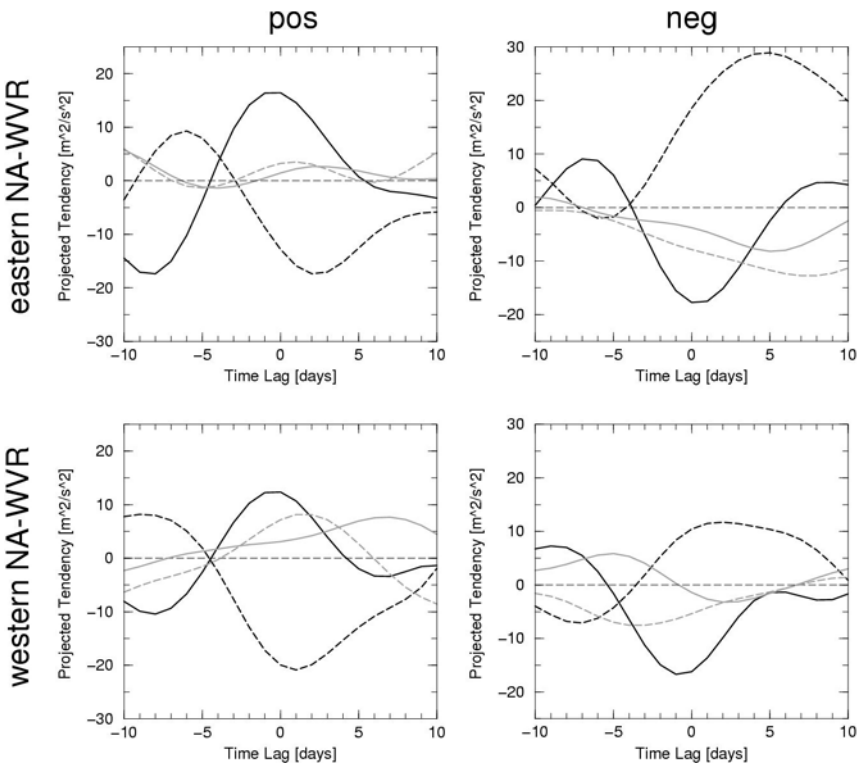

Figure 5. As in Figs. 4(c) and (d) but for persistent positive (left column) and negative (right column) episodes of the eastern NAT-WVR pattern index (upper row) and the western NAT-WVR pattern index (lower row).

anomaly (Figs. 4(c) and (d) and 5). The largest projection values can be observed during the growth phase, whereas they become small after the anomaly maximum. In most cases they only weakly contribute to its decay.

The contributions from transient eddies with different time-scales are presented in Figs. 4(e) and (f) for the NAT-SVR cases. The projections for the two NAT-WVR patterns are qualitatively similar and are therefore not shown. During anomaly growth, the forcing by low-frequency eddy vorticity fluxes, χ_5 (black dashed lines), is the dominant contributor to the total transient-eddy forcing and is always in phase with the latter. The interaction among the synoptic eddies, χ_6 (grey solid lines), also contributes to the anomaly growth but is less important than the low-frequency eddy forcing during times when the anomaly growth is most rapid. However, the synoptic-eddy forcing is still acting towards amplification of the stream function anomaly when the low-frequency eddy forcing has already reduced and changed its sign. This means that forcing by synoptic-eddy vorticity fluxes acts towards maintaining the anomaly after its maximum, whereas it plays a minor role during the anomaly growth.

In his examination of the NAO lifecycle, Feldstein (2003) also found high-frequency eddy forcing after the anomaly maximum. The contribution from the interaction of low-frequency and synoptic eddies, χ_7, is negligible (grey dashed lines in Figs. 4(e) and (f)). The sum of the projections of the terms χ_5, χ_6 and χ_7 is almost equal to the projection of the total transient-eddy forcing χ_{tr}. Thus, the contribution from eddies which were not captured by the time filters is small. The only exception is

the positive western NAT-WVR case, in which the contribution from eddies with periods between 6 and 10 days is somewhat larger and is in phase with the low-frequency eddy contribution (not shown).

Three terms have not been discussed yet: χ_1, χ_2 and χ_3. The sum of terms χ_1 and χ_2 describes the low-frequency advection of absolute vorticity due to the interaction of low-frequency eddies with the zonally symmetric part of the time-mean flow. The terms χ_1 and χ_2 force a westward (χ_1) or an eastward (χ_2) displacement of the stream function anomaly pattern (not shown). The single terms have large amplitudes but cancel each other to a large degree. It is therefore reasonable to discuss the sum of χ_1 and χ_2 rather than the single terms. From Figs. 4(c) and (d) and Fig. 5 it can be inferred that the net forcing contribution from combined terms χ_1 and χ_2 (grey dashed lines) is towards enhancing the stream function anomaly, except in the negative NAT-SVR index case where there is a weak damping contribution. The term χ_3 (grey solid lines) describes the forcing by low-frequency advection of relative vorticity resulting from the interaction of low-frequency eddies with the zonally asymmetric part of the time-mean flow, i.e. with the stationary eddies. It acts towards the growth of the stream function anomaly. Its contribution is largest a few days after the most rapid growth, as if to maintain the anomaly. If one compares the magnitudes of this forcing term and of the forcing by transient-eddy vorticity fluxes χ_{tr} (black solid lines), a considerable difference between the NAT-SVR and the NAT-WVR cases can be noticed: for the two NAT-WVR patterns, the transient-eddy vorticity fluxes χ_{tr} are the main contributor towards the growth of the stream function anomaly. In the NAT-SVR cases, however, the contributions from the two forcing terms χ_3 and χ_{tr} have almost equal magnitudes when the anomaly growth is most rapid (lag -1 day). In the positive NAT-SVR index case, term χ_3 becomes even larger afterwards. For the growth of a positive anomaly of NAT-SVR index, low-frequency eddies in interaction with stationary eddies dominate.

These analyses reveal that the growth of the teleconnection patterns identified in Fig. 1 is characterized by different physical mechanisms in the SVR and WVR. While the anomaly growth in the WVR is dominated by transient-eddy vorticity fluxes, in particular from the low-frequency domain, another forcing term is at least as important in the SVR: stream function tendency forcing by low-frequency vorticity advection due to the interaction of low-frequency eddies with the zonally asymmetric part of the time-mean flow, i.e. with the stationary eddies. This means that the different tropospheric teleconnection structures in the North Atlantic region are not just related to a spatial reorganization of the transient eddies in the different stratospheric regimes, but also to a modified interaction of (low-frequency) eddies with the changed background flow. The anomaly decay, however, is related to mainly the same forcing mechanisms in the two polar vortex regimes: the decay is dominated by forcing by the divergence term, whereas synoptic-eddy vorticity fluxes act towards maintaining the anomaly against decay.

Feldstein (2003) examined the life cycle of the NAO and found that it is mainly driven by forcing resulting from both low- and high-frequency eddy vorticity fluxes, whereas the decay is due to the influence of the divergence term and a (small) contribution from low-frequency eddy fluxes. These characteristics correspond to the life cycles of the two NAT-WVR patterns derived here. A possible explanation for the difference to the life cycle of the NAT-SVR pattern may be that, if the two regimes are not analysed separately, the differences between the mean flows in the two polar vortex regimes are incorrectly interpreted as low-frequency fluctuations. A part of the forcing which is related to the interaction between transient eddies and the time-mean flow within the polar vortex regimes is then interpreted as related to interactions among transient eddies. This shows the importance of the appropriate choice of analysis design.

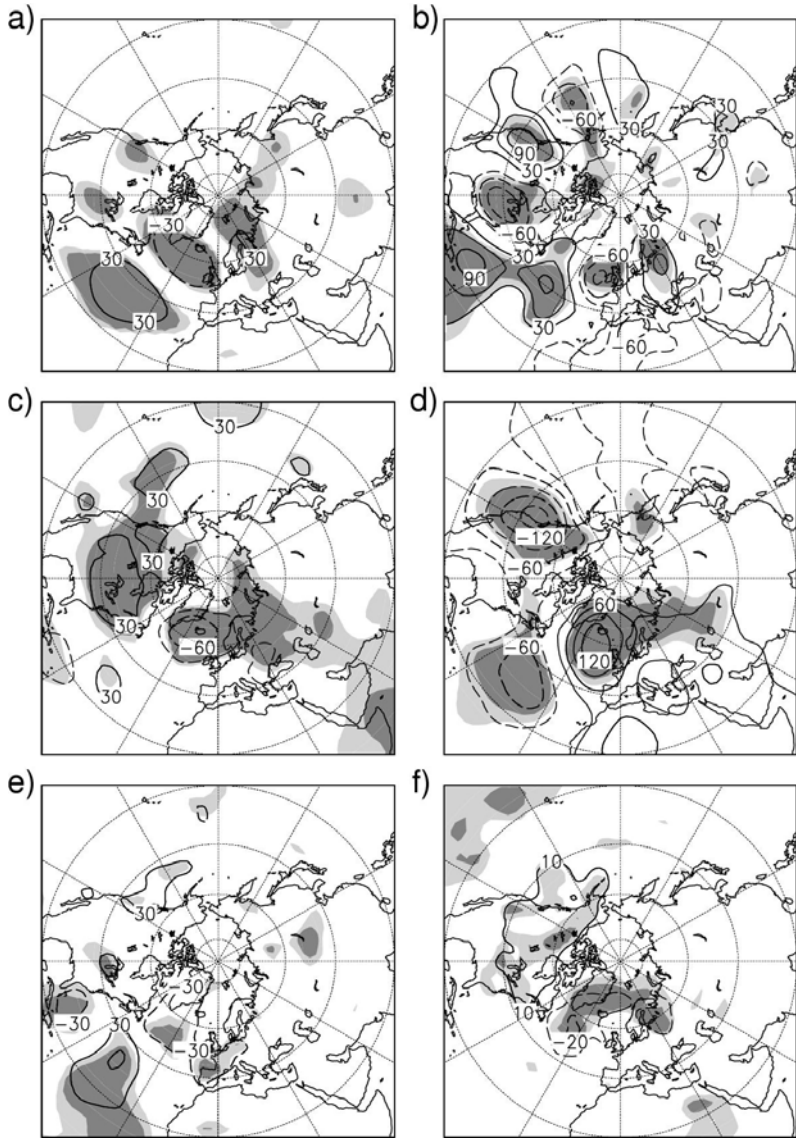

Figure 6. Composite low-pass-filtered 300 hPa stream function tendency and single terms in Eq. (1) (m^2s^{-2}) at lag -1 day for the positive persistent NAT-SVR pattern index episodes. Composites of (a) the total stream function tendency, (b) the sum of terms χ_1 and χ_2, (c) term χ_3, (d) term χ_4, (e) term χ_5 and (f) term χ_6. The isoline interval is 30 m^2s^{-2} in all panels except (f), where it is 10 m^2s^{-2}. The zero contours are omitted. The shadings indicate t-test significance above 95% (light shading) or 99% (dark shading).

In the following, spatial characteristics of the forcing terms in equation Eq. (1) are discussed. Two exemplary cases are illustrated for lag -1 day (i.e. one day before the maximum anomaly is reached), when the stream function tendency is maximum: Figure 6 displays composites for positive NAT-SVR index events and Fig. 7 composites for positive eastern NAT-WVR index events. Features described in the following are similar for all other teleconnection patterns and polarities.

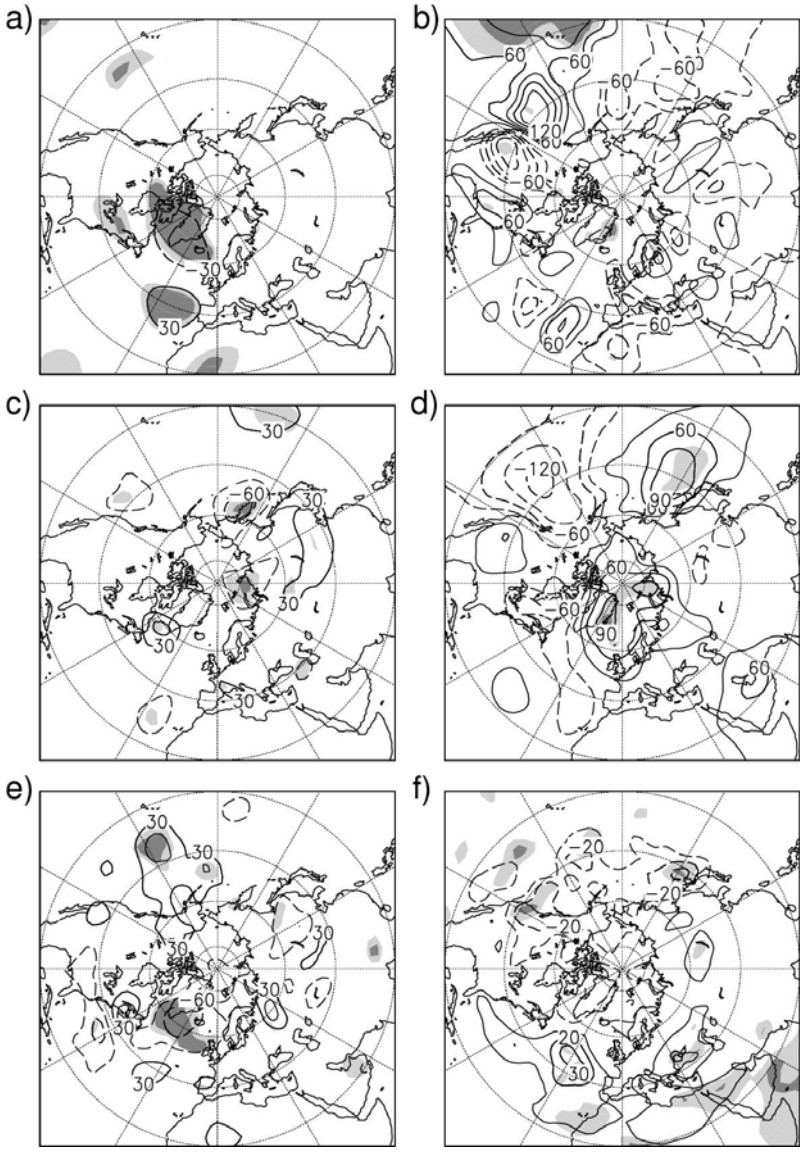

Figure 7. As in Fig. 6, but for the persistent positive eastern NAT-WVR pattern index episodes.

Figures 6(a) and 7(a) show the total stream function tendency. The structures are quite similar to the stream function anomaly during its mature stage (Fig. 3, lower left) and to the regression patterns in Fig. 1. The divergence term χ_4 has already been identified as the main contributor to the anomaly decay, whereas transient-eddy vorticity fluxes, χ_{tr}, appear to be important for the anomaly growth. This corresponds to the life cycle of the NAO (Feldstein 2003), whereas the growth of the Pacific/North American pattern is revealed to be mainly associated with forcing by interaction of low-frequency eddies with the time-mean flow (Feldstein 2002). Figures 6(d) and 7(d) show that the divergence term, χ_4, is clearly counteracting the total stream function tendency in both

centres of action of each teleconnection pattern. The damping by divergence is opposed in both centres of action by forcing due to transient-eddy vorticity fluxes, in particular from the low-frequency domain (Figs. 6(e) and 7(e)). The forcing by synoptic-eddy vorticity fluxes also acts to enhance the stream function anomaly (Figs. 6(f) and 7(f)). It is rather weak during the phase of the most rapid growth, i.e. for the time lag -1 day displayed in Figs. 6 and 7. However, as discussed previously, the magnitude of this forcing contribution increases as the stream function anomaly grows. The forcing by synoptic-eddy vorticity fluxes then acts towards maintaining the stream function anomaly against decay in both centres of action (not shown).

Turning back to the forcing resulting from the low-frequency eddy vorticity fluxes (Figs. 6(e) and 7(e)), it can be observed that it is more emphasized at the northern centre of action in the WVR than in the SVR. In the WVR, the growth of the northern centre of action is thus mainly driven by low-frequency eddy vorticity fluxes. In contrast, the deepening of the northern centre of action in the SVR is strongly driven by forcing induced by vorticity advection due to the interaction of low-frequency eddies with stationary eddies (Fig. 6(c)). The strength of the latter forcing contribution in the northern centre of action (of the NAT-SVR pattern) is associated with the intensified time-mean low near Greenland in the SVR, which is in turn maintained by stationary-eddy vorticity fluxes. The intensified time-mean low is related to strong time-mean vorticity gradients and wind anomalies leading to enhanced forcing due to vorticity advection near Iceland. While this forcing mechanism is strong for both polarities of the NAT-SVR pattern, its contribution hardly reaches the 95% significance level in the NAT-WVR cases (Fig. 7(c)).

The terms χ_1 and χ_2 describe low-frequency advection of absolute vorticity by interaction between low-frequency eddies and the zonally symmetric part of the time-mean flow, respectively. Together, they mainly force the growth of the subtropical centres of action (Figs. 6(b) and 7(b)). The forcing in the positive eastern NAT-WVR pattern case, however, is not significant above the 95% level and is much weaker than in the NAT-SVR cases. Comparison with the composite stream function anomalies for time lags -4 and 0 days (Fig. 3) exhibits that, in the positive NAT-SVR index case, there is also a contribution towards an eastward displacement of the subtropical high. This eastward movement has already been mentioned in the discussion of the development of the stream function anomalies. From Fig. 6(b), it becomes clear that the net influence from terms χ_1 and χ_2 is responsible for that. Such a displacement is not prominent in the negative NAT-SVR or in the NAT-WVR cases.

The structural differences between the North Atlantic teleconnection patterns in the two regimes of the stratospheric polar vortex strength cannot only be associated with a reorganization of transient eddies but also with different dynamical mechanisms. The latter is mainly related to the different stationary-eddy structures in the two regimes. Changes in the stationary-eddy structure have consequences for the interaction with transient eddies, and, thus, for the forcing in particular at the northern centre of action. This results in the strong wind anomalies over the northern North Atlantic in SVR (see Figure 2 in Graf and Walter 2005), in contrast to strong wind anomalies around the Azores High in WVR.

Figure 8 shows the eddy energy of low-pass (longer than 10 days) filtered 300 hPa geopotential heights for SVR and WVR. Clearly a positive anomaly can be identified over the central North Atlantic during SVR. It is produced by planetary wave reflection as was already shown by Perlwitz and Graf (2001) for zonal wave number one. It is suggested that this enhanced low-frequency variability contributes the differences in the life cycles of NAT in SVR and WVR by providing more low-frequency

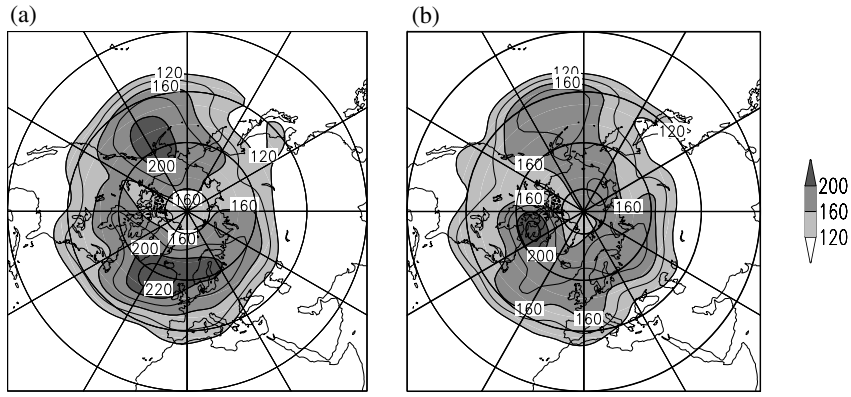

Figure 8. Root mean square of the low-pass (>10 days) filtered 300 hPa geopotential height (gpm) in (a) SVR and (b) WVR. For simplicity only values above 120 gpm are shown.

(including stationary) wave energy over the North Atlantic in SVR and giving more weight to χ_3 compared to χ_{tr}.

4. Conclusions

Teleconnections of North Atlantic geopotential heights were examined separately for winter months (December to March) characterized by either a strong or a weak stratospheric polar vortex. In both cases, the major teleconnection patterns have north–south dipole structures with opposing centres of action in subpolar and subtropic latitudes. The mid to upper troposphere in the strong vortex regime (SVR) is characterized by a single teleconnection pattern over the central North Atlantic with a basically dipolar structure, the NAT-SVR pattern. In contrast, there are two dipole patterns in the weak vortex regime (WVR): one over north-eastern Canada and the western North Atlantic (western NAT-WVR pattern) and a weaker one over the eastern North Atlantic (eastern NAT-WVR pattern). In the lower troposphere, however, the NAT-SVR and the eastern NAT-WVR patterns are very similar, in particular concerning their northern centres of action.

Fluctuations of the three North Atlantic teleconnection patterns have typical timescales of about two weeks. Life-cycle analyses of low-frequency (periods >10 days) stream function anomalies associated with the North Atlantic teleconnection patterns showed that the forcing mechanisms dominating the decay phase are basically the same in the two polar vortex regimes. The decay is mainly driven by low-frequency divergence whereas synoptic (periods 2.5 to 6 days) eddy vorticity fluxes act to maintain the anomaly against decay. However, the life-cycle analyses also revealed that, during the growth phase, the relative importance of the forcing mechanisms is very different in the two polar vortex regimes. In the WVR, the anomaly growth is mainly driven by transient-eddy vorticity fluxes, in particular from the low-frequency domain. In the SVR, however, a different forcing mechanism is of similar importance: the forcing related to low-frequency advection of (relative) vorticity which results from the interaction of low-frequency eddies with the zonally asymmetric part of the time-mean flow, i.e. with the stationary eddies. This means that the different teleconnection structures cannot simply be explained by a reorganization of the transient eddies in the different regimes but are also related to a modified interaction of the transient eddies with the

(changed) background flow. The latter can mainly be attributed to different stationary-eddy structures in the two polar vortex regimes during times when planetary wave energy is reflected back to the troposphere, i.e. during strong polar vortex episodes. It is suggested that these differences result in the preference of the positive NAO polarity during strong polar vortex episodes: growth of positive anomalies is enhanced by the stationary wave pattern resulting from planetary wave reflection, while the decay is not affected. Hence, there are fundamental differences in tropospheric dynamics associated with the generation of North Atlantic teleconnection patterns in the two stratospheric polar vortex regimes. The results may help us to understand the preferred NAO response to wave forcing when the polar vortex is strong. The reflection of wave energy leads to more low-frequency (including stationary) eddy energy over the North Atlantic and this contributes to the build-up of positive NAO phase. During non-reflective weak polar vortex episodes, zonal-mean anomalies can propagate down from the stratosphere leading to more zonally symmetric anomaly structures in the troposphere.

Acknowledgements

This work was sponsored by a PhD grant for KW under the AFO2000 KODYACS project of the German BMBF and by EU FW5 project PARTS.

References

Blackmon, M. L. and Lau, N.-C. 1980 Regional characteristics of the Northern Hemisphere wintertime circulation: A comparison of the simulation of a GFDL general circulation model with observations. *J. Atmos. Sci*., **37,** 497–514

Cai, M. and van den Dool, H. M. 1994 Dynamical decomposition of low-frequency tendencies. *J. Atmos. Sci.*, **51,** 2086–2100

Castanheira, J. M. and Graf, H.-F. 2003 North Pacific–North Atlantic relationships under stratospheric control? *J. Geophys. Res.*, **108,** 4036, doi: 10.1029/2002JD002754

Castanheira, J. M., Graf, H.-F., DaCamara, C. C. and Rocha, A. 2002 Using a physical reference frame to study global circulation variability. *J. Atmos. Sci.*, **59,** 1490–1501

Charney, J. G. and Drazin, P. G. 1961 Propagation of planetary-scale disturbances from the lower into the upper atmosphere. *J. Geophys. Res*., **66,** 83–109

Feldstein, S. B. 1998 The growth and decay of low-frequency anomalies in a GCM. *J. Atmos. Sci*., **55,** 415–428

2002 Fundamental mechanisms of the growth and decay of the PNA teleconnection pattern. *Q. J. R. Meteorol. Soc*., **128,** 775–796

2003 The dynamics of NAO teleconnection pattern growth and decay. *Q. J. R. Meteorol. Soc.*, **129,** 901–924

Feldstein, S. B. and Lee, S. 1996 Mechanisms of zonal index variability in an aquaplanet GCM. *J. Atmos. Sci*., **53,** 3541–3556

Graf, H.-F. and Walter, K. 2005 Polar vortex controls coupling of North Atlantic Ocean and atmosphere. *Geophys. Res. Lett.*, **32,** L01704, doi: 10.1029/2004GL020664

Hurrell, J. W., Kushnir, Y., Ottersen, G. and Visbeck, M. Eds. 2003 *The North Atlantic Oscillation: Climate significance and environmental impact*. Geophysical Monograph Series, **134**. American Geophysical Union

Kalnay, E., Kanamitsu, M., Kistler, R., Collins, W., Deaven, D., Gandin, L., Iredell, M., Saha, S., White, G., Woollen, J., Zhu, Y., Leetsmaa, A., Reynolds, B., Chelliah, M., Ebisuzaki, W., Higgins, W., Janowiak, J., Mo, K. C., Ropelewski, C., Wang, J., Jenne, R. and Joseph, D. 1996 The NCEP/NCAR 40-year reanalysis project. *Bull. Am. Meteorol. Soc*., **77,** 437–471

Kistler, R., Kalnay, E., Collins, W., Saha, S., White, G., Woollen, J., Chelliah, M., Ebisuzaki, W., Kanamitsu, M., Kousky, V., van den Dool, H., Jenne, R. and Fiorino, M. 2001 The NCEP–NCAR 50-year reanalysis: Monthly means CD-ROM and documentation. *Bull. Am. Meteorol. Soc.*, **82,** 247–267

Kodera, K. and Kuroda, Y. 2004 Two teleconnection patterns involved in the North Atlantic/Arctic Oscillation. *Geophys. Res. Lett.*, **31,** L20201, doi: 10.1029/2004GL020933

Perlwitz, J. and Graf, H.-F. 1995 The statistical connection between tropospheric and stratospheric circulation of the Northern Hemisphere in winter. *J. Climate*, **8,** 2281–2295

2001 Troposphere-stratosphere dynamic coupling under strong and weak polar vortex conditions. *Geophys. Res. Lett*., **28,** 271–274

Perlwitz, J. and Harnik, N. 2003 Observational evidence of a stratospheric influence on the troposphere by planetary wave reflection. *J. Climate*, **16,** 3011–3026

2004 Downward coupling between the stratosphere and troposphere: The relative roles of wave and zonal mean processes. *J. Climate*, **17,** 4902–4909

Wallace, J. M. and Gutzler, D. S. 1981 Teleconnections in the geopotential height field during the Northern Hemisphere winter. *Mon. Weather Rev*., **109,** 784–812

Walter, K. and Graf, H.-F. 2005 The North Atlantic variability structure, storm tracks, and precipitation depending on the polar vortex strength. *Atmos. Chem. Phys.*, **5,** 239–248. SRef-ID: 1680-7324/acp/2005-5-239